# A Simplified Fourier Method for Nonhydrostatic Mountain Waves

DAVE BROUTMAN

*Computational Physics, Inc., Springfield, Virginia*

JAMES W. ROTTMAN

*University of California, San Diego, La Jolla, California*

STEPHEN D. ECKERMANN

*Naval Research Laboratory, Washington, D.C.*

(Manuscript received 30 December 2002, in final form 24 April 2003)

ABSTRACT

A previously derived approximation to the standard Fourier integral technique for linear mountain waves is extended to include nonhydrostatic effects in a background flow with height-dependent wind and stratification. The approximation involves using ray theory to simplify the vertical eigenfunctions. The generalization to nonhydrostatic waves requires special treatment for resonant modes and caustics. Resonant modes are handled with a small amount of damping, and caustics are handled with a uniformly valid approximation involving the Airy function. This method is developed for both two- and three-dimensional flows, and its results are shown to compare well with an exact analytical result for two-dimensional mountain waves and with a numerical simulation for two- and three-dimensional mountain waves.

## 1. Introduction

The Fourier integral representation has been used in the linear modeling of mountain waves for over 50 yr and remains an important tool for mountain wave theory and forecasting (e.g., Vosper and Mobbs 1996; Smith et al. 2002; Shutts 1997). The representation is expressed as the inverse Fourier transform, over the horizontal wavenumbers, of the vertical eigenfunctions. Except for very special cases, the vertical eigenfunctions must be calculated numerically as the solution of a two-point boundary value problem. The numerical procedure is complicated by the presence of critical layers and trapped waves (e.g., Simard and Peltier 1982; Shutts 1997).

In Broutman et al. (2002) the authors simplified the calculation by approximating the vertical eigenfunctions with ray theory. We considered a slowly varying height-dependent background in the hydrostatic limit. Here, we extend this work to the nonhydrostatic case, which requires the treatment of trapped waves and the associated ray singularity at caustics.

The ray approximation for the vertical eigenfunctions is not to be confused with the ray approximation for the spatial wavefield. The latter has been computed for mountain waves by Broad (1999) and Shutts (1998), among others, and can be obtained in principal by the method of stationary phase. This is equivalent to taking an inverse Fourier transform of the vertical eigenfunctions and then finding the ray approximation. Here, we switch the order of these operations. That is, we find the ray approximation for the vertical eigenfunctions and then take an inverse Fourier transform. The order of operations makes an important difference for the solution near caustics.

A caustic is a singularity of ray theory that occurs where neighboring rays intersect each other, an extreme violation of the slowly varying approximation. For trapped waves, there can be numerous caustics in the lee of the mountain, which is why we do not calculate the spatial ray solution in the present paper. While these caustics are correctable with an Airy function, typically, the correction requires quantities that are not easily obtained unless the ray solution is known analytically.

The ray approximation for the vertical eigenfunctions also has caustics, and these too are correctable with an Airy function, typically. But the caustics for the vertical eigenfunctions and the caustics for the spatial ray approximation have different properties. For example, the caustics for the vertical eigenfunctions always occur at

*Corresponding author address:* Dave Broutman, E.O. Hulburt Center for Space Research, Naval Research Laboratory, 4555 Overlook Ave. S.W., Washington, DC 20375-5352.
E-mail: daveb@uap2.nrl.navy.mil

© 2003 American Meteorological Society

Unauthenticated | Downloaded 08/05/24 09:18 AM UTC

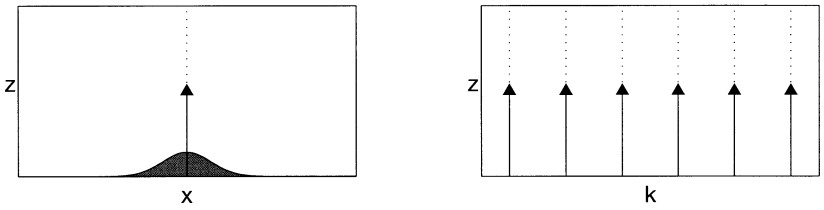


FIG. 1. Ray paths for Long's model all lie on the vertical axis above the mountain when plotted in the spatial domain (left) but are separated by horizontal wavenumber $k$ when plotted in the Fourier domain (right).

a buoyancy frequency turning point, while the caustics for the spatial ray approximation *never* occur at a buoyancy frequency turning point. We explain why and show an example in section 3—see the description of Fig. 2.

Most importantly, the correction of the caustics for the vertical eigenfunctions is a one-dimensional analysis. This simplifies the calculation, compared with the multidimensional case for the spatial caustics. Thus, the procedure we use is to compute the ray approximation for the vertical eigenfunctions, correcting for caustics in a standard way with the Airy function. An inverse Fourier transform of the result then gives the spatial solution, which is valid at all of the spatial caustics without further correction.

The present approach is related to Maslov's method, developed in the 1960s by V. P. Maslov (e.g., Maslov and Fedoriuk 1981; Kravtsov and Orlov 1999). In Maslov's method, caustics in the spatial domain are avoided by using the inverse Fourier transform of the ray solution from the Fourier domain. In our problem, the ray solution from the Fourier domain is just the ray solution for the vertical eigenfunctions. The hydrostatic mountain wave theory of Shutts (1998) is an example of this approach, as we discussed in Broutman et al. (2002). We have since noticed that a similar idea was suggested for mountain waves by Miles (1969), though the relevant expression given by Miles in his Eq. (4.13) does not apply to trapped waves.

The strength of Maslov's method is how it deals with nonseparable problems, which lack an eigenfunction representation. Maslov's method combines ray solutions from the Fourier and spatial domains using Fourier transforms, in such a way that the local caustic correction functions, like the Airy function, are never needed. Brown (2000) gives an example. The same procedure could be used here, but since our problem has an eigenfunction representation, it is natural to use an Airy function for the caustics in the Fourier domain because, as we noted above, the analysis in the Fourier domain is a simple one-dimensional calculation.

One way to derive the ray approximation for the vertical eigenfunctions is by an asymptotic analysis of the vertical structure equation, given in general form and in several limits by Inverarity and Shutts (2000). This is the approach used by Shutts (1998) and Miles (1969). Another derivation, which is used here and leads to the same result, is to ray trace in the Fourier domain, as we did in Broutman et al. (2002) for the hydrostatic case. This approach is applicable to more general backgrounds, for example, with horizontal variability, but mostly we use it because such an alternate derivation helps to enhance the understanding of the results.

To analyze trapped waves, it is convenient to start with the case of uniform stratified hydrostatic flow over topography in a channel (section 2). The trapping is imposed by the rigid upper lid. This is Long's model, and the present analysis leads to a new derivation of the linearized limit of Long's solution. We can easily extend the derivation to the case of nonhydrostatic waves in a height-dependent background without an upper boundary. This is done in section 3.

In section 4 we show that the present method compares well with the two-dimensional theory of Wurtele et al. (1987) based on the exact vertical eigenfunctions. In section 5 we give a three-dimensional example. Throughout the paper we use the Boussinesq approximation, and we ignore the effects of the earth's rotation.

## 2. Long's hydrostatic channel model

A simple demonstration of the present method for the case of trapped waves is provided by Long's model of flow over topography in a channel. Long's model (Long 1955; Baines 1995) is hydrostatic and steady state, with constant mean flow $U$ and constant mean-buoyancy frequency $N$. The topography $z = h(x)$ is localized, with $h \to 0$ as $x \to \pm\infty$. The upper boundary of the channel is at $z = D$.

### *a. Rays in the spatial domain*

The rays in the spatial domain all emerge from a single point at the center of the topography. [This point source of rays is a feature of radiation from a localized source and can be justified by a stationary-phase approximation, as in Shutts (1998).] The rays then propagate straight upward along the vertical axis above the mountain (Fig. 1, left). The rays cannot spread laterally in the hydrostatic limit because the upstream intrinsic group speed of the waves is perfectly balanced by the downstream flow. Nor can the rays reflect laterally from the mountain after a round trip to the top of the channel

Unauthenticated | Downloaded 08/05/24 09:18 AM UTC

and back. Even if the mountain were sloped at the point where the rays return to it, the rule for internal waves is that the rays preserve their angle with respect to the vertical upon reflection. Thus the rays reflect straight upward again. Without any lateral dispersion, the slowly varying approximation fails completely and the spatial ray solution predicts a vertical displacement amplitude that is infinite at any point on the vertical axis and that is zero at any point off the vertical axis.

### b. Rays in the Fourier domain

We can make more progress with ray theory if we express the ray solution as a function of the horizontal wavenumber $k$ and the depth $z$. This is the Fourier domain for this problem. The depth is treated parametrically and is not transformed.

For Long's model, the rays that line up on the vertical axis above the mountain in the spatial domain are separated in the Fourier domain by their values of $k$, as illustrated in the right side of Fig. 1. There is still an infinite number of rays of the same $k$ at each $z$, due to the continual generation of rays at the lower boundary and the continual reflection of rays by both boundaries. It is, however, possible to sum the contributions from all rays of the same $k$, as we now show.

Let $\hat{\omega}$ be the intrinsic frequency, with $\hat{\omega} = -kU$ for stationary waves. We assume that $U$ is positive and that $k$ is negative. The hydrostatic dispersion relation gives the vertical wavenumber magnitudes as $m = |k|N/\hat{\omega}$, which after substituting for $\hat{\omega}$ becomes $m = N/U$.

The ray solution for the vertical displacement in the Fourier domain will be represented by $\tilde{\eta}(k, z)$. The boundary conditions are

$$\tilde{\eta}(k, 0) = \tilde{h}(k), \qquad \tilde{\eta}(k, D) = 0, \tag{1}$$

where $\tilde{h}(k)$ is the Fourier transform of $h(x)$.

We derive the ray solution for $\tilde{\eta}(k, z)$ by tracing rays in the Fourier domain. We start with some initial ray generated at $z = 0$ and ignore all rays generated previously. That is, we consider an initial value problem without the complication of transients and look for the long-time solution. Just before the initial ray reaches the upper boundary for the first time, the ray solution is

$$\tilde{\eta}^{(0)} = \tilde{h}(k)e^{-imz}. \tag{2}$$

The zero superscript indicates that no reflections have occurred yet. With notation $m > 0$, the negative sign in the phase indicates a downward phase velocity and an upward group velocity. After the initial ray has its first reflection at the top boundary, but just before it has its second reflection at the bottom boundary the ray solutions is

$$\tilde{\eta}^{(1)} = \tilde{h}(k)e^{-imz} - \tilde{h}(k)e^{im(z-2D)}. \tag{3}$$

The second term represents downward-moving rays and combines with the first term to satisfy the upper boundary condition.

Just before the initial ray reaches the upper boundary for the second time, after one reflection from the upper boundary and one reflection from the lower boundary, the ray solution is

$$\tilde{\eta}^{(2)} = \tilde{h}(k)e^{-imz} - \tilde{h}(k)e^{im(z-2D)} + \tilde{h}(k)e^{-im(z+2D)}. \tag{4}$$

The third term is the same as the first term except for the phase shift of $-m2D$, resulting from a difference in the length of the propagation path.

Each incident ray combines with its reflected ray to nullify the vertical displacement at the boundary. The upper boundary condition is thus satisfied pairwise. The lower boundary condition is thus satisfied by the single ray being generated for the first time at the mountain and represented in the first term on the right in (2), (3), and (4).

The continued reflections generate an infinite number of rays that superimpose at each $z$. We represent this for the upward-moving rays by

$$\tilde{\eta}_{\text{up}}(k, z) = \tilde{h}e^{-imz}S, \tag{5}$$

and for the downward-moving rays by

$$\tilde{\eta}_{\text{dn}}(k, z) = -\tilde{h}e^{im(z-2D)}S, \tag{6}$$

with

$$S = \sum_{n=0}^{\infty} e^{-in2mD}. \tag{7}$$

For a fixed $z$, each term in the sum for $\tilde{\eta}_{\text{up}}$ and each term in the sum for $\tilde{\eta}_{\text{dn}}$ differs only by a phase shift, an integer multiple of $-m2D$.

The sum $S$ is divergent in the strict sense, since the terms do not vanish as $n \to \infty$, but it does converge in the sense of generalized functions. From Hardy [1949, their Eq. (1.2.2)],

$$S = (1 - i\,\cot mD)/2 = -ie^{imD}/2\,\sin mD. \tag{8}$$

The total vertical displacement thus becomes

$$\begin{aligned}\tilde{\eta}(k, z) &= \tilde{\eta}_{up} + \tilde{\eta}_{dn} \\ &= \tilde{h}e^{-imD}[e^{-im(z-D)} - e^{im(z-D)}]S \\ &= \frac{\tilde{h}\,\sin m(D - z)}{\sin mD}.\end{aligned} \tag{9}$$

The spatial solution is now obtained by inverse Fourier transform:

$$\begin{aligned}\eta(x, z) &= \int_{-\infty}^{\infty} \tilde{\eta}(k, z)e^{ikx}\,dk \\ &= \frac{\sin m(D - z)}{\sin mD}\int_{-\infty}^{\infty} \tilde{h}(k)e^{ikx}\,dk \\ &= h(x)\,\frac{\sin m(D - z)}{\sin mD}.\end{aligned} \tag{10}$$

This is Long's solution for small-amplitude topography (see p. 279 of Baines 1995).

Unauthenticated | Downloaded 08/05/24 09:18 AM UTC

### 3. Two-dimensional theory for U(z), N(z)

We now remove the rigid lid of section 2 and examine a two-dimensional model in which the waves are nonhydrostatic and trapped by variations in the background wind and stratification. The generalization to three dimensions is straightforward (section 5). We develop the theory for a height-dependent mean wind $U(z)$ and mean buoyancy frequency $N(z)$. The nonhydrostatic dispersion relation is

$$\hat{\omega} = \pm kN/(k^2 + m^2)^{1/2}. \tag{11}$$

For stationary waves $\hat{\omega} = -kU$. We assume slowly varying waves, except near caustics. This limits the strength of variations in $U(z)$, $N(z)$ (see, e.g., section 3c of Broutman et al. 2002).

As in section 2, we use an infinite sum to represent the multiply reflected rays in the Fourier domain. The theory of section 2 needs to be modified for the present model to account for refraction in a height-dependent background and to account for the phase shift from a buoyancy frequency turning point.

First we consider the wave amplitude. In section 2, each ray has a constant vertical-displacement amplitude $\tilde{h}(k)$ in the Fourier domain—see Eqs. (5)–(7). For a height-dependent background, this must be modified to conserve the vertical flux of wave action for each $k$. Defining

$$G \equiv N^2 c_{g3}/\hat{\omega}, \tag{12}$$

the wave-action flux is $G|\tilde{\eta}|^2$. Enforcing the lower boundary condition $\tilde{\eta} = \tilde{h}$ at $z = 0$ gives

$$|\tilde{\eta}| = \tilde{h}[G_0/G]^{1/2}, \tag{13}$$

where $G_0 = G(z = 0)$.

Next we consider the wave phase. The channel height $D$ in Long's model is replaced by the turning point height $z_t$, which is a function of $k$. The generalization of the wave phase in (5)–(6) is the standard one in which $mz$ becomes the phase integral $\int_0^z m\,dz$, and accordingly $mD$ becomes $\int_0^{z_t} m\,dz$. There is a phase shift at the turning point $z_t$, and this enters into the generalization of $S$ in (7), as we now discuss.

Following a ray through one round-trip to the top of the channel and back led, in section 2, to a decrease in the wave phase by an amount $-2mD$. Actually there are phase shifts of $\pi$ at both the upper and lower boundaries, but this contributes an additional factor of $2\pi$ to the phase of $S$ and so can be ignored. In the present generalization we still have the phase shift of $\pi$ at the lower boundary, but the upper boundary is a buoyancy-frequency turning point, and this introduces a different phase shift which we call $\alpha$, for now. Thus $2mD$ in (7) becomes $2\int_0^{z_t} m\,dz + \alpha + \pi$.

Summarizing, the generalization of the ray solution from Long's model is then, in (5)–(6),

$$\tilde{h} \to \tilde{h}[G_0/G]^{1/2}, \tag{14}$$

$$mz \to \int_0^z m\,dz, \tag{15}$$

$$mD \to \int_0^{z_t} m\,dz, \tag{16}$$

and in (7),

$$2mD \to 2\int_0^{z_t} m\,dz + \alpha + \pi. \tag{17}$$

Making these substitutions, and continuing in the same way as the derivation that leads to (9), gives

$$\tilde{\eta}(k, z) = \tilde{h}\left[\frac{G_0}{G}\right]^{1/2} \frac{\sin[\Gamma - \chi(z)]}{\sin\Gamma}, \tag{18}$$

where

$$\chi = \int_0^z m(z')\,dz', \tag{19}$$

$$\Gamma = \chi(z_t) + \alpha/2 + \pi/2. \tag{20}$$

Long's solution for $\hat{\eta}$ in (9) is recovered from (18) by setting $\alpha = \pi$ (the phase shift for reflection from a solid boundary), and by letting $\chi = mz$ and $G/G_0 = 1$ (as they are for a uniform medium).

Equation (18) applies only to those $k$ values that have turning points. For the $k$ values without turning points we use the formula derived in Broutman et al. [2002, their Eq. (26)]. In present notation, this is

$$\tilde{\eta}(k, z) = \tilde{h}(G_0/G)^{1/2} \exp[-i\int_0^z m(k, z')\,dz'], \tag{21}$$

which represents only upward-moving rays.

The inverse Fourier transform (10) of (18), and possibly of (21), gives the spatial solution for $\eta(x, z)$. But there are two singularities to deal with before this can provide a meaningful result. The first is $G = 0$, which occurs when $c_{g3} = 0$ and corresponds to either a critical layer or a turning point. We dealt with the critical layer in Broutman et al. (2002) by simply filtering out Fourier components of large vertical wavenumber. That worked effectively, at least for the model considered in that paper. Now we must deal with the turning point singularity, which is a caustic in the Fourier domain. The other singularity of (18) is $\Gamma = n\pi$, for integer $n$, which occurs when reflecting rays of the same $k$ have perfect constructive interference.

#### a. Caustics

The standard correction procedure for a caustic is to match the ray solution to an Airy function $\mathrm{Ai}(\rho)$ in its asymptotic form for large negative $\rho$ (Bender and Orszag 1978):

Unauthenticated | Downloaded 08/05/24 09:18 AM UTC

$$\mathrm{Ai}(\rho) \approx \pi^{-1/2}|\rho|^{-1/4} \sin\left[\frac{2}{3}|\rho|^{3/2} + \frac{\pi}{4}\right]. \qquad (22)$$

The caustic height $z = z_t$ corresponds to $\rho = 0$, with $\rho > 0$ ($z > z_t$) in the "shadow" zone and $\rho < 0$ ($z < z_t$) in the "lit" zone. The relation between $\rho$ and $z$ is

$$\frac{2}{3}|\rho|^{3/2} = \int_z^{z_t} m(z')\, dz' = \chi(z_t) - \chi(z)$$

$$= \Gamma - \frac{1}{2}(\alpha + \pi) - \chi(z). \qquad (23)$$

Setting the previously undetermined phase shift at the caustic to $\alpha = \pi/2$ gives

$$\frac{2}{3}|\rho|^{3/2} + \frac{\pi}{4} = \Gamma - \chi(z), \qquad (24)$$

so the sine functions in the Airy function formula (22) and in the ray solution (18) have the same argument, as required.

The matching of the ray solution to the Airy function is a well-known procedure, but we will use an alternate description that gives a uniform approximation, that is, a single expression valid close to and far from the caustic. This approach is generally more accurate than the matching method. A discussion of the uniform approximation for the one-dimensional Helmholtz equation is given in Bender and Orzsag (1978, p. 510), and for a more general case, by Kravtsov and Orlov (1999). The uniform solution, derived in the appendix, is

$$\tilde{\eta}_u = \tilde{h}\left[\frac{G_0^2\rho}{G^2\rho_0}\right]^{1/4} \frac{\mathrm{Ai}(\rho)}{\mathrm{Ai}(\rho_0)}. \qquad (25)$$

The zero subscript means an evaluation at $z = 0$. The factor of $G^{-1/2}$ causes the ray solution (18) to be singular at the caustic, but in (25) that singularity is canceled by the factor $|\rho|^{1/4}$. The spatial solution is now

$$\eta(x, z) = \int_{-\infty}^{\infty} \tilde{\eta}_u(k, z) e^{ikx}\, dk. \qquad (26)$$

### *b. Resonant modes, $\Gamma = n\pi$*

In the Fourier domain, the total phase change $2\Gamma$ along the ray in one round-trip from the ground to the turning point and back again (including the phase shifts at the caustic and at the ground) can turn out to be an integer multiple of $2\pi$. We then have a resonant mode in which there is perfect constructive interference between all rays of the same $k$. In Long's model, all modes have the same resonant condition $mD = n\pi$ for integer $n$—see (10). There is no linear steady-state solution in that case. In the present model, the resonant condition is different for each $k$, and each gives rise to an integrable pole in the inverse Fourier transform, as in Eq. (7) of Wurtele et al. (1989).

We remove the singularity associated with the resonant modes by adding a small amount of damping in the form of an imaginary part for $k$. We discuss the effectiveness of this damping in the next section. (See the description of Fig. 4.)

## 4. Comparison with Wurtele et al. (1987)

Wurtele et al. (1987), hereafter WSK, have analyzed two-dimensional mountain waves in a mean wind given by

$$U = U_0 Z, \qquad Z = 1 + z/L, \qquad (27)$$

where $U_0$ and $L$ are constants. We consider the tropospheric model in WSK section 2a. The topography used by WSK is

$$h(x) = h_0 a^2/(x^2 + a^2), \qquad (28)$$

where $a$ is a constant. The Fourier transform of $h$ is

$$\tilde{h} = h_0 a e^{-a|k|} \qquad (29)$$

In the following we use the parameter values of WSK's case II, which are $N = 0.01\ \mathrm{s}^{-1}$ and

$$a = 2.5\ \mathrm{km}, \qquad h_0 = 100\ \mathrm{m}, \qquad L = 4.0\ \mathrm{km},$$

$$U_0 = 10\ \mathrm{m\ s}^{-1}. \qquad (30)$$

Figure 2 shows ray paths for this model, plotted as a function of their spatial-domain coordinates (top) and as a function of their Fourier-domain coordinates (bottom). The spatial rays originate at the origin and are calculated from an integration of the standard ray equations (Lighthill 1978). The corresponding rays in the two domains can be identified by the height of their turning points, which are the same in the two domains. In the Fourier domain the rays follow a straight vertical line because $k$ is constant along the ray in a horizontally uniform background.

In the Fourier domain, the turning point is a caustic. Neighboring rays of the same $k$, generated at slightly different times, intersect as they reflect from the turning point. The intersection of neighboring rays is what defines a caustic. In the spatial domain the turning point is not a caustic. This is most clear at the first downwind occurrence of turning points in the top of Fig. 2. The rays arc back toward the ground without intersecting. Caustics form for a particular ray only after that ray reflects once from the ground. Four caustics are discernible in the top of Fig. 2 as approximately straight lines that slope upward with increasing $x$. Each caustic is an envelop for the rays that intersect it, and each ray intersects its caustic before reaching its turning point.

The turning point in the spatial domain is never a caustic in this model. To understand why, note that each ray is uniquely determined by its position $(x, z)$ and by its horizontal wavenumber $k$. At a caustic in the spatial domain, the intersecting rays must by definition have the same value of $x$ and $z$. At a caustic in the Fourier

Unauthenticated | Downloaded 08/05/24 09:18 AM UTC

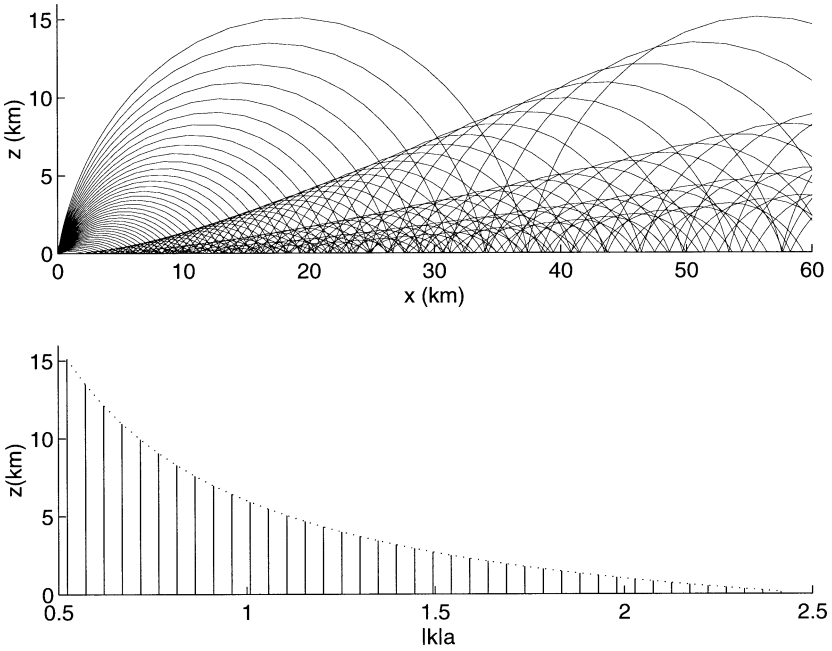


FIG. 2. Corresponding ray paths in the spatial domain (top) and in the Fourier domain (bottom) for the model of section 4. The values for the horizontal wavenumber $k$ correspond to horizontal wavelengths ranging from 6.5 to 30 km. In the bottom, the $k$ axis is normalized by the mountain width $a = 2.5$ km, and the dotted line indicates the turning-point height.

domain, the intersecting rays must by definition have same value of $k$ and $z$. If the ray intersections were to happen at the same $z$ in both domains, the intersecting rays would then have the same values of $x$, $z$, and $k$, and thus would not be distinct.

The exact vertical eigenfunctions for the WSK model involve Bessel functions, as contained in WSK's Eq. (6). Converting their expression from perturbation streamfunction to vertical displacement and removing their non-Boussinesq mean-density scaling, the WSK eigenfunctions become

$$\tilde{\eta}_{\mathrm{WSK}}(k, z) = h_0 a Z^{1/2} e^{-|k|a} \frac{K_{i\mu}(kLZ)}{K_{i\mu}(kL)}. \qquad (31)$$

Here, $\mu = N^2L^2/U_0^2 - 1/4$, and $K_{i\mu}$ is the modified Bessel function of imaginary order.

Our $\tilde{\eta}_u(k, z)$ in (25) is an approximation for the exact vertical eigenfunction (31). Tests of this approximation are shown in Fig. 3, in which we plot the exact eigenfunction (31), the uniform approximation (25), and the singular ray solution (18). Each of the three panels corresponds to a different value of $k$, as labeled by the horizontal wavelength $\lambda = 2\pi/|k|$. The agreement between the exact vertical eigenfunction and the uniform approximation is close, with the case of $\lambda = 40$ km showing the largest discrepancy. The size of the discrepancy is related to the nearness of the vertical eigenfunction to a resonant mode. At resonance the vertical eigenfunction diverges, and the difference between the exact and approximate values is accentuated, as we show next.

In Fig. 4, the uniform approximation and the exact vertical eigenfunction are plotted as a function of $|k|a$ at a height corresponding to $\rho = -1$, close to the depth at which the vertical eigenfunctions have their local maximum nearest the caustic. Resonance occurs at $\lambda$ approximately equal to 15 and 36 km, or $|k|a \approx 1.05$ and $|k|a \approx 0.44$, respectively.

The uniform approximation in Fig. 4 is calculated with an imaginary part $k_i = 5 \times 10^{-6}\ \mathrm{m}^{-1}$ added to the real part of $k$. The only significant effect of $k_i$ is on those eigenfunctions that are near resonance. The asterisks show the three values of $ka$ corresponding to Fig. 3, which was also computed with $k_i = 5 \times 10^{-6}$. From left to right in Fig. 4, the asterisks denote the values $\lambda = 40$, 20, 10 km. The accuracy of the uniform approximation in Fig. 4 is seen to depend on the nearness of $\lambda$ to a resonant value.

Note that by damping the near-resonant modes preferentially, as indicated by Fig. 4, we damp the waves of the far field preferentially. In the far field, the resonant modes make the dominant contribution to the wave field, as noted in WSK's discussion of their Eq. (7). In the near field, a wide range of eigenfunctions contributes significantly to the solution. Thus damping the near-resonant modes has less of an effect on the near-field solution than on the far-field solution.

The value of $k_i = 5 \times 10^{-6}\ \mathrm{m}^{-1}$ is used to generate

Unauthenticated | Downloaded 08/05/24 09:18 AM UTC

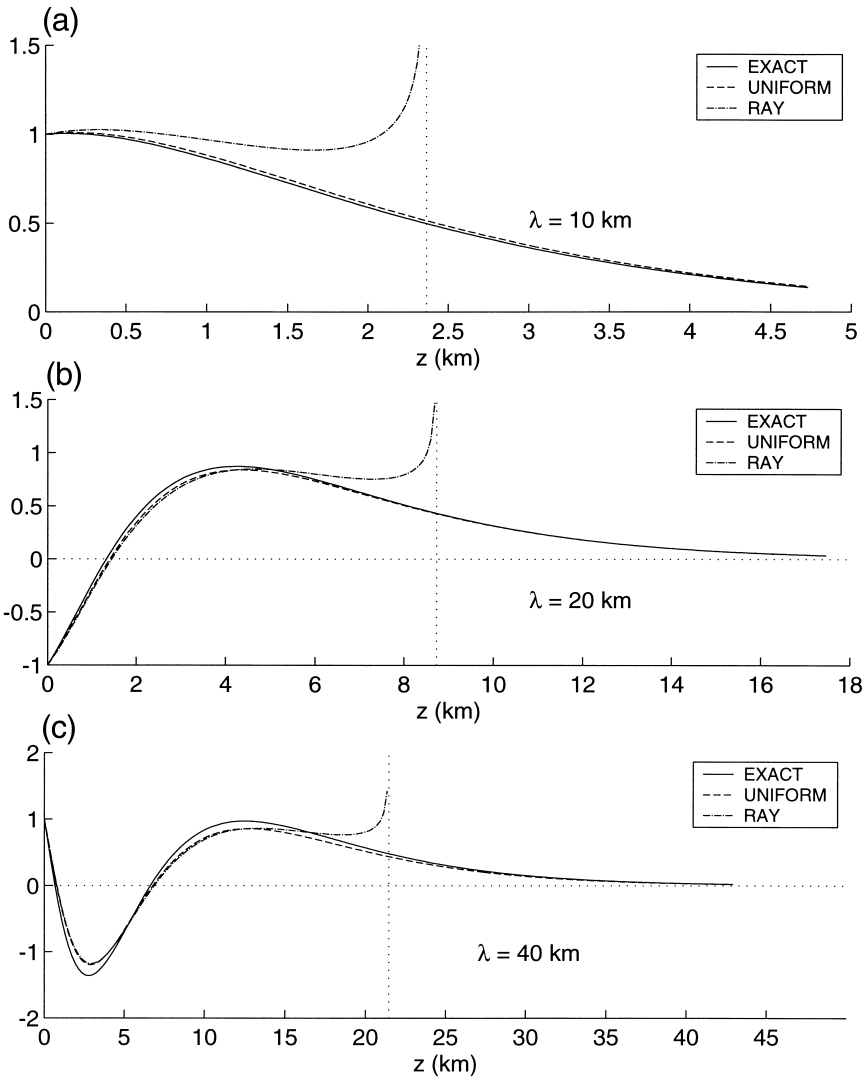


FIG. 3. A comparison of the exact vertical eigenfunction (31), the uniform approximation (25), and the ray approximation (18). The solutions are normalized by $\tilde{h}(k)$. Three cases are given for different values of $\lambda = 2\pi/|k|$. The vertical dotted line indicates the turning-point height, where the ray approximation diverges. Parameter values are given in (30).

the results plotted in this paper and corresponds to a horizontal decay scale $k_i^{-1}$ of 200 km. We chose this value specifically for the WSK model, in which the mountain width is only 2.5 km. More generally, we would choose the value of $k_i$ in order to damp the far-field waves sufficiently so that periodic wrap-around errors are not important. Periodic wrap-around errors result from the approximation of the inverse Fourier transform (26) by a finite Fourier series (as described in, e.g., Broutman et al 2002). Note that periodic wrap-around errors in the discrete approximation of the inverse Fourier transform also occur when the exact vertical eigenfunctions are used (e.g., Shutts 2001). For the two-dimensional case in Fig. 5, to be discussed next, we found that changing $k_i^{-1}$ from 200 to 1000 km increased the maximum wave amplitudes by about 15%. For the three-dimensional case of Fig. 6, the same change in $k_i^{-1}$ increased the maximum wave amplitudes by about 5%.

In Fig. 5, we plot the solution for the vertical velocity predicted by the present simplified Fourier method. This is computed using the ray-approximated vertical eigenfunction $\tilde{w}(k, z) = ikU\tilde{\eta}_u(k, z)$. The result agrees well with the result of a numerical model, which is also shown in Fig. 5. The numerical model is a standard one: it is nonlinear, Boussinesq, and discretized with second-order finite differences. The lower boundary is free slip, and the flow is turned on instantly to full strength at the initial time. The results are plotted after 15 h of simulation time, when an approximate steady state is achieved. The numerical model has a domain size of 130 km by 52 km, with a grid spacing of 1 km in each

Unauthenticated | Downloaded 08/05/24 09:18 AM UTC

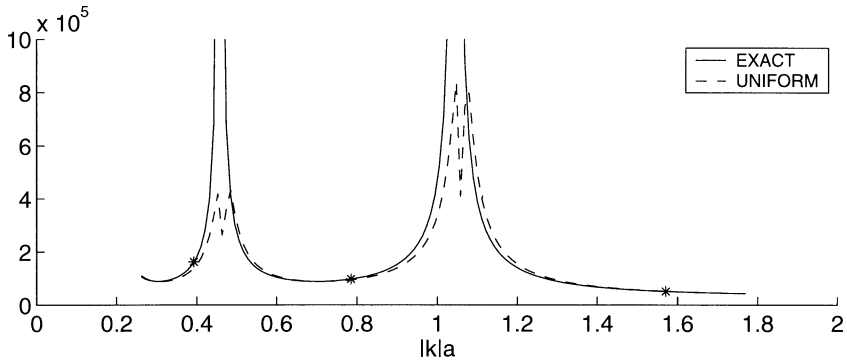


FIG. 4. The exact vertical eigenfunction (31) and the uniform approximation (25) as a function of $|k|a$ at a depth corresponding to the Airy function variable $\rho = -1$. The uniform calculation has an imaginary wavenumber $k_i = 5 \times 10^{-6}$ m$^{-1}$. The exact calculation is for $k_i = 0$. The left, center, and right asterisks correspond respectively to $\lambda = 40$, 20, 10 km, the values used in Fig. 3.

direction. A sponge is in effect from about $x > 80$ km and $z > 35$ km. The results from this numerical model are similar to those obtained by numerical simulation in Fig. 9 of WSK. [Our magnitudes are lower than those plotted in Figs. 2 and 9 of WSK by a factor of about 5. We have concluded that there is a minor error in the labeling of these two figures in WSK since we have verified our results with two different numerical models and an evaluation of WSK's far-field approximation (7).]

## 5. A three-dimensional example

We now use the notation $x$, $y$, $z$ for the spatial coordinates and $k$, $l$, $m$ for the wavenumber coordinates. The background wind has components $U$ in the $x$ direction and $V$ is the $y$ direction. The dispersion relation is

$$\hat{\omega} = k_h N/(k_h^2 + m^2)^{1/2}, \tag{32}$$

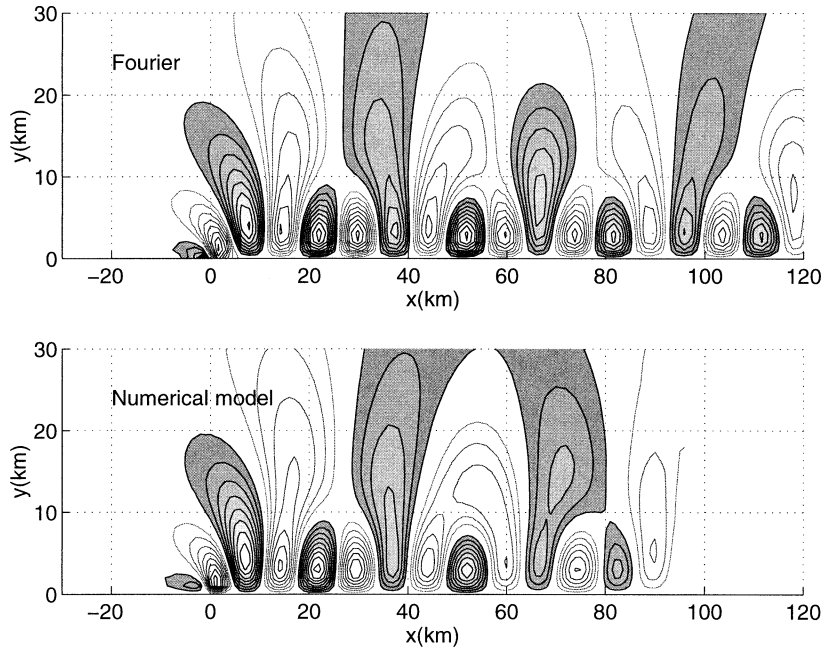


FIG. 5. The vertical velocity for the WSK model predicted by the present simplified Fourier method (top) and by a numerical simulation (bottom). The contour interval in both plots is 0.04 m s$^{-1}$, with positive contours shaded and the zero contour omitted. Values range from $-0.37$ to 0.38 m s$^{-1}$ for the Fourier method and from $-0.34$ to 0.38 m s$^{-1}$ for the numerical model. The Fourier solution is calculated at heights of every kilometer from the ground to an altitude of 30 km. At each height, 256 horizontal wavenumbers are used. The corresponding spatial domain has a horizontal periodic length of about 804 km and a horizontal grid spacing of about 1.57 km. The numerical model has 130 points in the horizontal and 52 points in the vertical, with a grid spacing of 1 km in both directions.

Unauthenticated | Downloaded 08/05/24 09:18 AM UTC

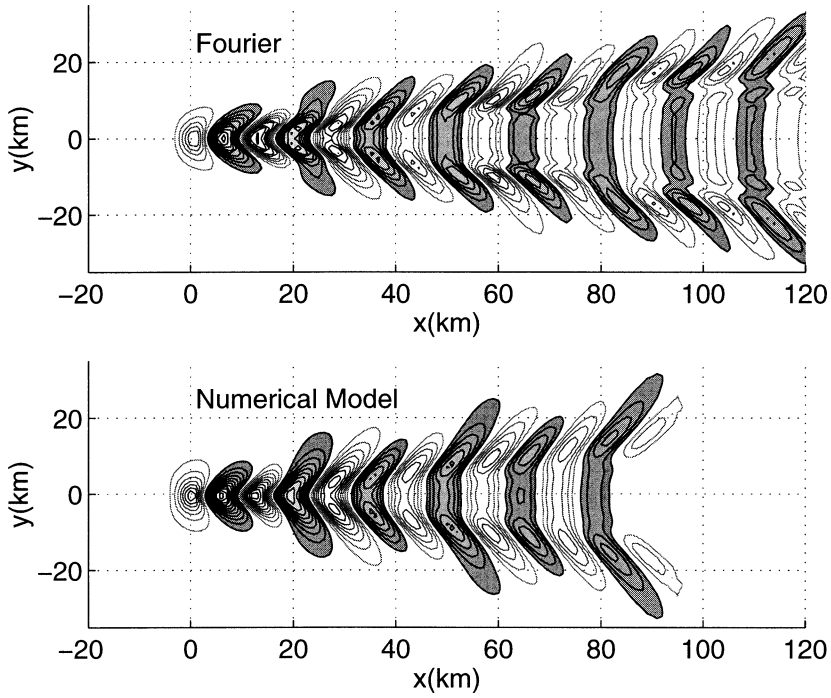


FIG. 6. The vertical velocity at $z = 2.5$ km computed by the present simplified Fourier method (top) and by a numerical model (bottom). The contour interval is 0.02 m s$^{-1}$, with positive contours shaded and the zero contour omitted. Values range from $-0.18$ to 0.21 for the present method, and from $-0.21$ to 0.25 for the numerical model. A sponge is used in the numerical model beyond about $x = 80$ km.

where $k_h = (k^2 + l^2)^{1/2}$. For stationary waves $\hat{\omega} = -kU - lV$.

The uniform approximation (25) is applicable to the three-dimensional case after the simple modification of including the dependence on $l$ in $\tilde{h}(k, l)$, $m(k, l, z)$, etc., and in the inverse Fourier transform

$$\eta(x, y, z) = \int_{-\infty}^{\infty}\int_{-\infty}^{\infty} \tilde{\eta}(k, l, z)e^{i(kx+ly)}\, dk\, dl. \quad (33)$$

Similarly, the expression (21) for those Fourier components without turning points applies to the three-dimensional case when the $l$ dependence is included.

For an example we consider the WSK model with parameters given by (30) and $V = 0$. The topography is now three-dimensional:

$$h(x, y) = h_0 a^2/(x^2 + y^2 + a^2)^{3/2}, \quad (34)$$

with Fourier transform

$$\tilde{h}(k, l) = \frac{1}{2\pi} h_0 a^2 e^{-k_h a}. \quad (35)$$

All Fourier components have turning points, except those with $k = 0$, for which $\hat{\omega} = 0$. We ignore these components.

The vertical velocity is contoured in Fig. 6 at a height of 2.5 km. The top of Fig. 6 shows the solution from the present Fourier method, and the bottom shows the results of a numerical simulation. The numerical model is the same one used to produce the results in Fig. 5, with the additional detail that the grid spacing in $y$ is 1 km, as it is in $x$ and $z$. For the Fourier method, 256 wavenumbers are used in $k$ and $l$. The corresponding spatial domain has a horizontal periodic length of about 670 km and a horizontal grid spacing of about 1.31 km.

## 6. Final comments

The usual Fourier integral representation for mountain waves in a height-dependent background has been simplified by replacing the exact vertical eigenfunctions with their ray approximation. An Airy function correction removes the singularity associated with caustics and a small amount of damping (in the form of an imaginary part of the wavenumber) removes the singularity associated with resonant modes. The main result is given by (25), whose inverse Fourier transform is the spatial mountain wave solution.

Because of its reliance on the ray approximation, the present method does not account for partial reflection from gradual changes in the background. In addition, the Airy function representation used here fails in some cases. For example, if the mean wind in the model of section 4 were replaced by a jet-shaped profile, then caustics near the tip of the jet would not be described

Unauthenticated | Downloaded 08/05/24 09:18 AM UTC

by an Airy function but by a parabolic cylinder function [or Weber function; see Kravtsov and Orlov (1999)].

The effects of the earth's rotation have also been omitted. Shutts (2001) includes rotation in a mountain wave model, using a Fourier method with the exact vertical eigenfunctions for a particular mean-wind profile. One computational issue is that an infinitely long train of near-inertia waves forms in the lee of the mountain, which gives periodic wrap-around errors in the discrete approximation of the inverse Fourier transform. This is the same problem we have encountered here with the resonant trapped modes (see the discussion surrounding Fig. 4), and Shutts uses a similar fix. He adds a small imaginary component to the intrinsic frequency, which damps the near-inertia waves and limits their horizontal extent. We have used this damping and the ray approximation for Shutts' vertical eigenfunctions to approximately reproduce Fig. 6 of Shutts (2001), but we have not made more thorough tests with rotation.

*Acknowledgments.* We thank John Lindeman for providing the numerical simulations presented in Figs. 5 and 6. SDE acknowledges support for this research from the Office of Naval Research. SDE and DB also acknowledge support from NASA's Office of Space Science through the Geospace Science Program (Grant W19862). Additional support was received from the National Science Foundation under Grant OCE-0117869.

## APPENDIX

### Derivation of the Uniform Approximation (25)

We follow the method of Kravtsov and Orlov (1999, section 10.1.3). The ray solution is of the form

$$U = U_1 e^{i\phi_1} + U_2 e^{i\phi_2}, \tag{A1}$$

and the uniform approximation is of the form

$$u = \pi^{1/2}[A\mathrm{Ai}(\rho) + iB\mathrm{Ai}'(\rho)]e^{i\xi}. \tag{A2}$$

Here, Ai is the Airy function and the prime means differentiation with resect to $\rho$. The Airy function is a good approximation of the linear solution near the caustic. The idea of the uniform approximation is to modify the argument and amplitude of the Airy function so that it also fits the linear solution at distances farther away from the caustic.

A comparison of (A1) with the far-field asymptotic form of (A2) leads Kravtsov and Orlov to the following:

$$\xi = \frac{1}{2}(\phi_1 + \phi_2), \tag{A3}$$

$$\frac{2}{3}(-\rho)^{3/2} = \frac{1}{2}(\phi_1 - \phi_2), \tag{A4}$$

$$A = (-\rho)^{1/4}(iU_1 + U_2)e^{-i\pi/4}, \tag{A5}$$

$$B = (-\rho)^{1/4}(iU_1 - U_2)e^{-i\pi/4}. \tag{A6}$$

The ray solution with $U_1$ and $\phi_1$, corresponds to the ray incident on the caustic, while the ray solution with $U_2$ and $\phi_2$ corresponds to ray reflected from the caustic. For our problem, the incident and reflected rays have the same amplitude dependence on height, so $|U_1| = |U_2|$, but there is a phase shift of $+\pi/2$ upon reflection (section 3). Thus, $U_2 = U_1 \exp(i\pi/2)$, or $iU_1 = U_2$, which gives $B = 0$. For our problem,

$$\phi_1 = -\phi_2 = -\int_z^{z_t} |m|\, dz, \tag{A7}$$

where we have written the phase relative to the caustic height $z_t$. This gives $\xi = 0$, and the uniform approximation reduces to

$$u = -i(2\pi)^{1/2}(-\rho)^{1/4}U_1\mathrm{Ai}(\rho). \tag{A8}$$

If $U$ represents the vertical displacement, then by conservation of wave action $|U_1|$ is proportional to $G^{-1/2}$, where $G = N^2 c_{g3}/\hat{\omega}$ was introduced in (12). It remains only to apply the boundary conditions at $z = 0$. We could do that for the ray solution $U$ or, more directly now, for the uniform approximation $u$. The result is (25); that is,

$$u = \tilde{h}\left[\frac{G_0^2\rho}{G^2\rho_0}\right]^{1/4}\frac{\mathrm{Ai}(\rho)}{\mathrm{Ai}(\rho_0)}. \tag{A9}$$

The zero subscripts indicate evaluation at $z = 0$, and $\tilde{h}$ is the Fourier transform of the topography.

## REFERENCES

Baines, P. G., 1995: *Topographic Effects in Stratified Fluids.* Cambridge University Press, 482 pp.

Bender, C. M., and S. A. Orszag, 1978: *Advanced Mathematical Methods for Scientists and Engineers.* McGraw-Hill, 593 pp.

Broad, A., 1999: Do orographic gravity waves break in flows with uniform wind direction turning with height? *Quart. J. Roy. Meteor. Soc.*, **125,** 1695–1714.

Broutman, D., J. W. Rottman, and S. D. Eckermann, 2002: Maslov's method for stationary hydrostatic mountain waves. *Quart. J. Roy. Meteor. Soc.*, **128,** 1159–1172.

Brown, M. G., 2000: The Maslov integral representation of slowly varying dispersive wave-trains in inhomogeneous moving media. *Wave Motion,* **32,** 247–266.

Hardy, G. H., 1949: *Divergent Series.* Clarendon, 396 pp.

Inverarity, G. W., and G. J. Shutts, 2000: A general, linearized vertical structure equation for the vertical velocity: Properties, scalings, and special cases. *Quart. J. Roy. Meteor. Soc.*, **126,** 2709–2724.

Kravtsov, Y. A., and Y. Orlov, 1999: *Caustics, Catastrophes, and Wave Fields.* Springer, 216 pp.

Lighthill, M. J., 1978: *Waves in Fluids.* Cambridge University Press, 504 pp.

Long, R. R., 1955: Some aspects of the flow of stratified fluids. III. Continuous density gradients. *Tellus,* **7,** 341–357.

Maslov, V. P., and M. E. Fedoriuk, 1981: *Semi-Classical Approximation in Quantum Mechanics.* D. Reidel, 301 pp.

Miles, J. W., 1969: Waves and wave drag in stratified flows. *Proceedings of the 12th International Congress of Applied Mechanics,* M. Hetenyi and W. Vincenti, Eds., Springer-Verlag, 50–76.

Shutts, G. J., 1997: Operational lee wave forecasting. *Meteor. Appl.,* **4,** 23–35.

Unauthenticated | Downloaded 08/05/24 09:18 AM UTC

——, 1998: Stationary gravity-wave structure in flows with directional wind shear. *Quart. J. Roy. Meteor. Soc.*, **124,** 1421–1442.
——, 2001: A linear model of back-sheared flow over an isolated hill in the presence of rotation. *J. Atmos. Sci.*, **58,** 3293–3311.
Simard, A., and W. R. Peltier, 1982: Ship waves in the lee of isolated topography. *J. Atmos. Sci.*, **39,** 587–609.
Smith, R. B, S. T. Skubis, J. D. Doyle, A. Broad, C. Kiemle, and H. Volkert, 2002: Mountain waves over Mt. Blanc: Influence of a stagnant boundary layer. *J. Atmos. Sci.*, **59,** 2073–2092.
Vosper, S. B., and S. D. Mobbs, 1996: Lee waves over the English Lake District. *Quart. J. Roy. Meteor. Soc.*, **122,** 1283–1305.
Wurtele, M. G., R. D. Sharman, and T. L. Keller, 1987: Analysis and simulations of a troposphere–stratosphere gravity wave model. Part 1. *J. Atmos. Sci.*, **44,** 3269–3281.

Unauthenticated | Downloaded 08/05/24 09:18 AM UTC